Available online at www.sciencedirect.com
ScienceDirect
Aerosol Science 38 (2007) 592–603
Journal of Aerosol Science
www.elsevier.com/locate/jaerosci

Generation of C_{60} nanoparticle aerosol in high mass concentrations

Amit Gupta*, William C. Forsythe, Mark L. Clark, Jeffrey A. Dill, Gregory L. Baker

Battelle Toxicology Northwest, 900 Battelle Boulevard, Richland, Washington, USA

Received 2 January 2007; received in revised form 12 April 2007; accepted 1 May 2007

Abstract

The generation of nanoparticles at concentrations sufficient to perform toxicology studies is highly challenging. The vaporization/condensation technique has successfully been used previously to generate nanoparticle aerosol. However, the maximum mass concentrations generated were low ($\sim 0.180\,\mu g/L$), and the generation method produced aerosol having a mixed chemical composition. In this study, a new, dynamically operated, nanoparticle generation system has been developed that generates nanoparticles having a count median diameter of 40–60 nm and continuously delivers a mass concentration as high as $2\,\mu g/L$ at the nose exposure port of a nose only exposure system. This system generated nanoparticles by using an inline tube furnace for flash vaporizing micron-sized particles fed continuously from an aerosol generator. This paper describes both the experiments and the operating conditions used for generating nanoparticles to demonstrate the system's capability and the methods used for physicochemical characterization of the resulting nanoparticles.
© 2007 Elsevier Ltd. All rights reserved.

Keywords: Nanoparticles; C_{60}; Buckminsterfullerenes; High concentration; Inhalation toxicology

1. Introduction

Nanomaterials exhibit novel and enhanced properties because of their unique physical and chemical behavior. Consequently, nanotechnology has the potential to make significant contributions in many fields, from semiconductors to biotechnology to energy, transportation, agriculture, food and consumer products (Hood, 2004). Nanomaterials have been used for decades in products such as paint pigments, resins and cosmetics (The National Nanotechnology Initiative, 2006). The presence of nanoparticles in the environment has also been confirmed from natural sources such as fires, volcanoes, sea spray, erosion or anthropogenic sources such as traffic, industry and cigarette smoke (Borm et al., 2006). Inhalation is considered the most significant exposure route for these unintentionally generated nanoparticles (Oberdorster, Oberdorster, & Oberdorster, 2005; Oberdorster et al., 2005). In addition to specifically engineered nanomaterials, an estimated 50,000 kg/year of nanosized materials are being produced through unintended anthropogenic sources such as diesel exhaust and other combustion sources (Borm et al., 2006). Regulatory agencies have mainly focused on particulate matter $< 10\,\mu m$ in diameter (PM_{10}) and $< 2.5\,\mu m$ in diameter ($PM_{2.5}$), but there is evidence that adverse health effects are higher for the finer particle fraction (Borm et al., 2006; Colvin, 2003). Improvements in measurement techniques have focused attention more recently on ultrafine particles whose diameter

* Corresponding author. Tel.: +1 509 375 2560; fax: 1 509 375 3649.
E-mail address: guptaamit@battelle.org (A. Gupta).

0021-8502/$ - see front matter © 2007 Elsevier Ltd. All rights reserved.
doi:10.1016/j.jaerosci.2007.05.002

$< 0.1\ \mu m$ ($PM_{0.1}$) is consistent with nanoparticle definitions (MacNee & Donaldson, 2000; Oberdorster, Oberdorster et al., 2005).

Recent advancements in technology and understanding of materials behavior at the nanoscale level have enhanced the capabilities to reproducibly generate engineered nanoparticles with specific chemical and physical properties (Joutsensaari et al., 1996). An inventory of manufacturer self-identified consumer products compiled by the Project on Emerging Nanotechnologies has identified more than 300 nanoproducts already available in the market worldwide (Taylor, 2006). Although current production of engineered nanomaterials is relatively small, it is evident that as a result of increased R&D investments, production will accelerate in the next few years. Such products have far-ranging applications in cosmetics, foods and food packaging, medical products, microelectronics, transportation and a host of other areas of great importance to consumers, public health, the economy and the environment.

The extraordinary pace of innovation in nanotechnology has raised huge concerns as to how the safety of nanotechnology is regulated and how the products made of nanomaterials are seen and accepted by the public (Gerritzen, Huang, Killpack, Holden, & Harthorn, 2006; Meili, 2006). There are several specific factors that are likely to lead to toxicity peculiar to nanomaterials (Cheng, 2004; Oberdorster, Oberdorster et al., 2005). Nanoparticles can access regions of the body that may not be accessible by larger particles. Evidence exists that some nanoparticles have the potential to cross the blood-brain barrier (Kreuter, 2001) and leak out of capillaries. Nanomaterials may enter the body via mechanisms different than those used by larger particles (e.g., diffusion) and may bypass common clearance pathways for particulate matter. Also, nanomaterials have very high surface-to-volume ratios; their high surface-free energy leads to facile adsorption of molecular contaminants, offering a potential route for such contaminants into regions of the body not normally accessible. Some studies have even suggested the total surface area of the retained particles as the best dose–response parameter for incidence of lung tumors (Oberdorster, 1996).

The initial discovery of Buckminsterfullerene, C_{60} (commonly called buckyballs), has stimulated a multitude of research involving this special allotrope of carbon (Kroto, Heath, O'Brien, Curl, & Smalley, 1985). Because of its unique physical and chemical properties, there are numerous potential applications of C_{60} nanoparticles in industry including optical devices, chemical sensors, batteries, hydrogen storage, drug delivery systems, polymers, plastics and catalysts. Fullerene manufacturing facilities throughout the world anticipate total production to be several thousand tons by 2007 (Borm et al., 2006). Much of the previous documented work in laboratory aerosol generation of buckyballs was directed towards characterizing their various properties such as phase, crystallinity, reactivity, geometry, physical and chemical properties (McCready & Alnajjar, 1993). Fullerenes can also be coated at the time of production with a variety of biocompatible materials, but it is unknown how long these coatings will stay with the fullerene moiety during weathering in an environmental setting and what will happen to the fullerenes once the coating is removed.

The generation of nanoparticulate aerosol of C_{60} fullerenes for inhalation toxicology studies is highly challenging. Aerosol concentrations for inhalation toxicology exposures are typically much higher than $1\ \mu g/L$. Due to their high surface area, nanoparticles tend to form agglomerates, thus increasing their particle size and reducing their number concentration. An aerosol generation system for inhalation toxicology exposures must be able to reproducibly generate nanoparticulate aerosol in relatively high mass concentrations, and the particle size must remain stable over the duration of exposures. Since the mass associated with nanoparticles is very small, chemical characterization of the exposure atmosphere to ensure the chemical purity of the exposed chemical at the exposure port is also challenging. Characterization of the distribution, elimination and overall fate of nanoparticulates in exposed mammalian test systems can also be quite difficult.

Previous approaches to generate C_{60} nano-sized aerosol include nebulizing a toluene solution of C_{60} with subsequent vaporization and condensation of the aerosol stream to break the huge aggregates (Joutsensaari et al., 1996). The difficulty with this approach for inhalation exposure is the simultaneous generation of toluene, which must be completely separated from the aerosol. Another approach involves using arc discharge between graphite electrodes to generate carbon vapor. Besides C_{60}, this vapor consists of other higher molecular weight fullerenes (C_{70}, C_{84}, etc.) and amorphous carbon (Kroto et al., 1985). Because the objective of the present study was to create an aerosol atmosphere that can be used for health and safety testing of C_{60} nanoparticulates, these approaches were ruled out.

In this study, we describe an engineering system that we designed and built to continuously generate stable C_{60} nanoparticle aerosol at relatively high mass concentration for evaluating potential health effects in inhalation toxicology studies.

2. Materials and methods

A schematic of the system used to generate the C_{60} aerosol is depicted in Fig. 1. Bulk C_{60} was purchased from SES Research (Houston, TX) and was milled (Wig-L-Bug, Crystal Laboratories, Garfield, NJ) prior to use. The generation system consisted of a rotary dust feeder (Battelle Toxicology Northwest, Richland, WA), connected to a single-jet Particle Attrition Chamber (PAC, Battelle Toxicology Northwest, Richland, WA). A puff of compressed nitrogen aerosolized the bulk C_{60} powder from the metering port of the rotary dust feeder to the PAC inlet. The PAC used a pressurized nitrogen jet to promote particle-to-particle impaction, thus breaking apart the particles. The aerosol flow exiting the PAC was siphoned off such that ~0.400 lpm entered a quartz tube positioned within a tube furnace (Barnstead International Model F21135). C_{60} aerosol passing through the quartz furnace tube (maintained at 550 °C) was flash vaporized.

The furnace has a chamber length of 12 in (30.8 cm) and a tube diameter of 2 in (5.08 cm) into which a quartz tube of similar dimensions was placed. It has been reported that there may be some thermophoretic losses in a laminar flow reactor caused by temperature gradients at the inlet and outlet of the reactor (Damour, Ehrman, Karlsson, & Karlsson, 2005). The quartz tube was designed to minimize any such losses to the walls of the tube. The furnace tube consists of a vaporization chamber and a dilution chamber. Compressed nitrogen was introduced in the dilution chamber to cool and dilute the supersaturated vapor and reduce the residence time to minimize the particle agglomeration during the condensation process. Several experiments were conducted at various temperatures to observe the effect of temperature on the chemical integrity of C_{60} fullerenes. The nanometer-sized aerosol exiting the furnace tube was diluted with compressed air to achieve the desired level of oxygen (>19.5%) for inhalation exposures. An on–off exposure valve directed the aerosol to the nose-only exposure carousel during the on-exposure period and toward the house vacuum through a HEPA filter during the off-exposure period.

Samples of C_{60} nanoparticulate aerosol were collected from a nose port of the exposure carousel and were subjected to physical and chemical analysis. The size distribution of the generated aerosol was determined using a scanning

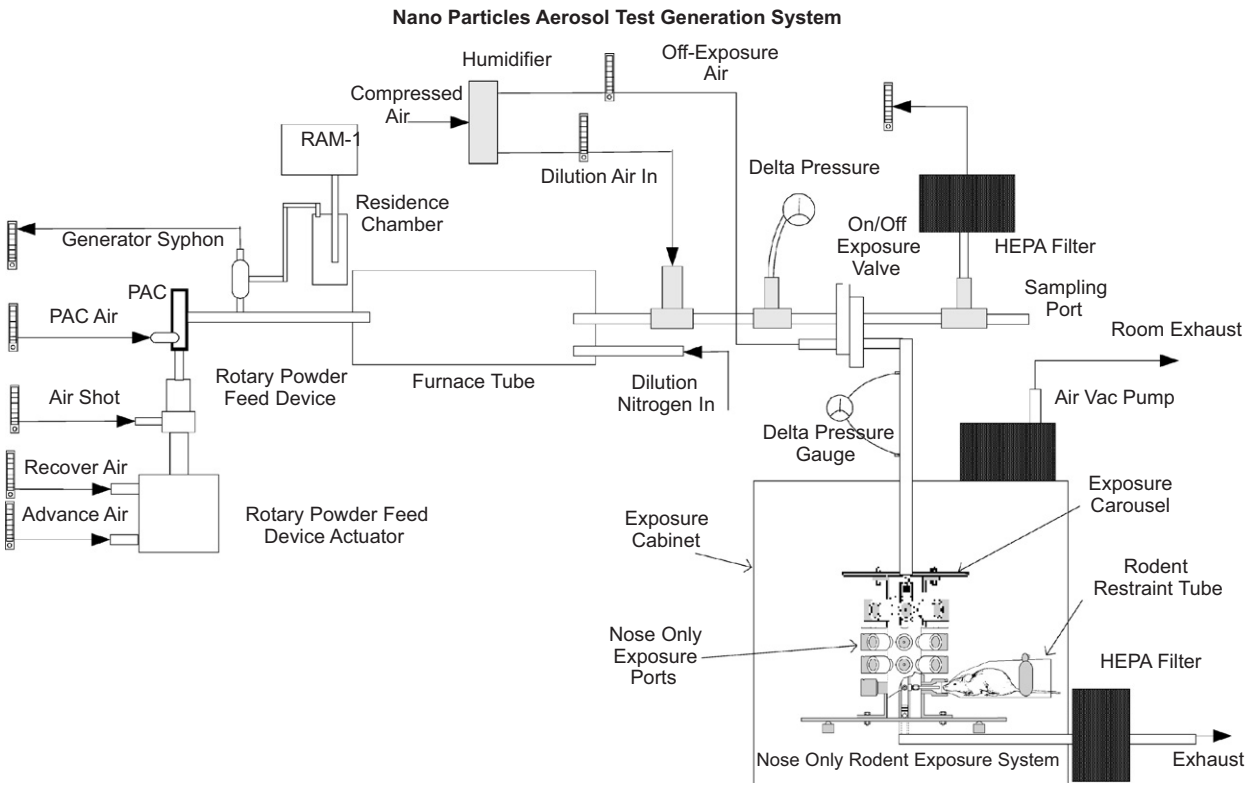

Fig. 1. Schematic diagram of the system to aerosolize C_{60}.

Table 1
Representative SMPS data for a 3-min sample

Parameter	Num. particle size
Count median diameter (nm)	53
Count mean diameter (nm)	55
Geometric mean (nm)	50
Mode (nm)	58
Geometric standard deviation	1.53
Total concentration	8.20e06 (#/cm^3)

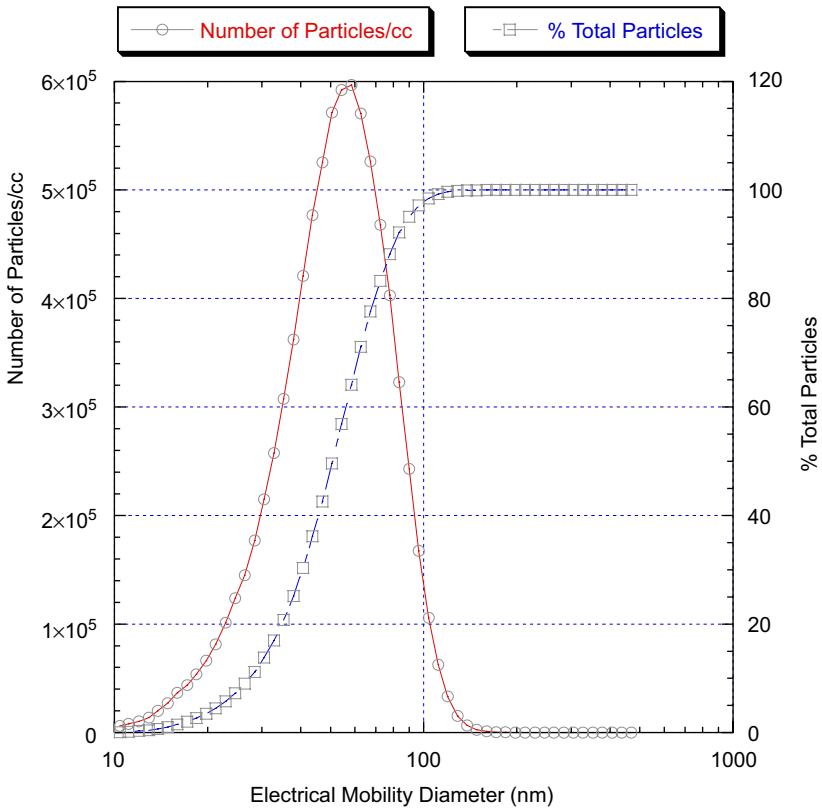

Fig. 2. Representative concentration (y_1-axis) and percent total particles (y_2-axis) versus diameter (x-axis) as observed.

mobility particle sizer (SMPS; TSI Model 3034), scanning electron microscope (SEM) imaging (SEM, LEO 982 FE-SEM, Zeiss), transmission electron microscope (TEM) imaging (JEOL 2010F) and Micro-orifice uniform deposit impactor (MOUDI) (MSP Corp, 125B NanoMOUDI). The chemical characterization of C_{60} was performed using laser Raman spectroscopy (Spex Model 1877), X-ray diffraction (XRD) (40 kV, 30 mA, CuK$_\alpha$, Germany) and high-performance liquid chromatography (HPLC, Agilent 1100).

The SMPS samples were collected from the nose port of the exposure carousel and were used to size, separate and count particles on the basis of their electrical mobility. The SEM images of bulk C_{60} particles were taken by collecting the aerosol samples at the output of the PAC. For SEM analysis, aerosol samples were collected on a gold-plated 25-mm membrane filter (Pal Gelman, MI). The TEM images of nano- and micro-sized C_{60} aerosol were taken by collecting the aerosol samples from the nose port of the exposure carousel. For TEM, the samples were collected on a

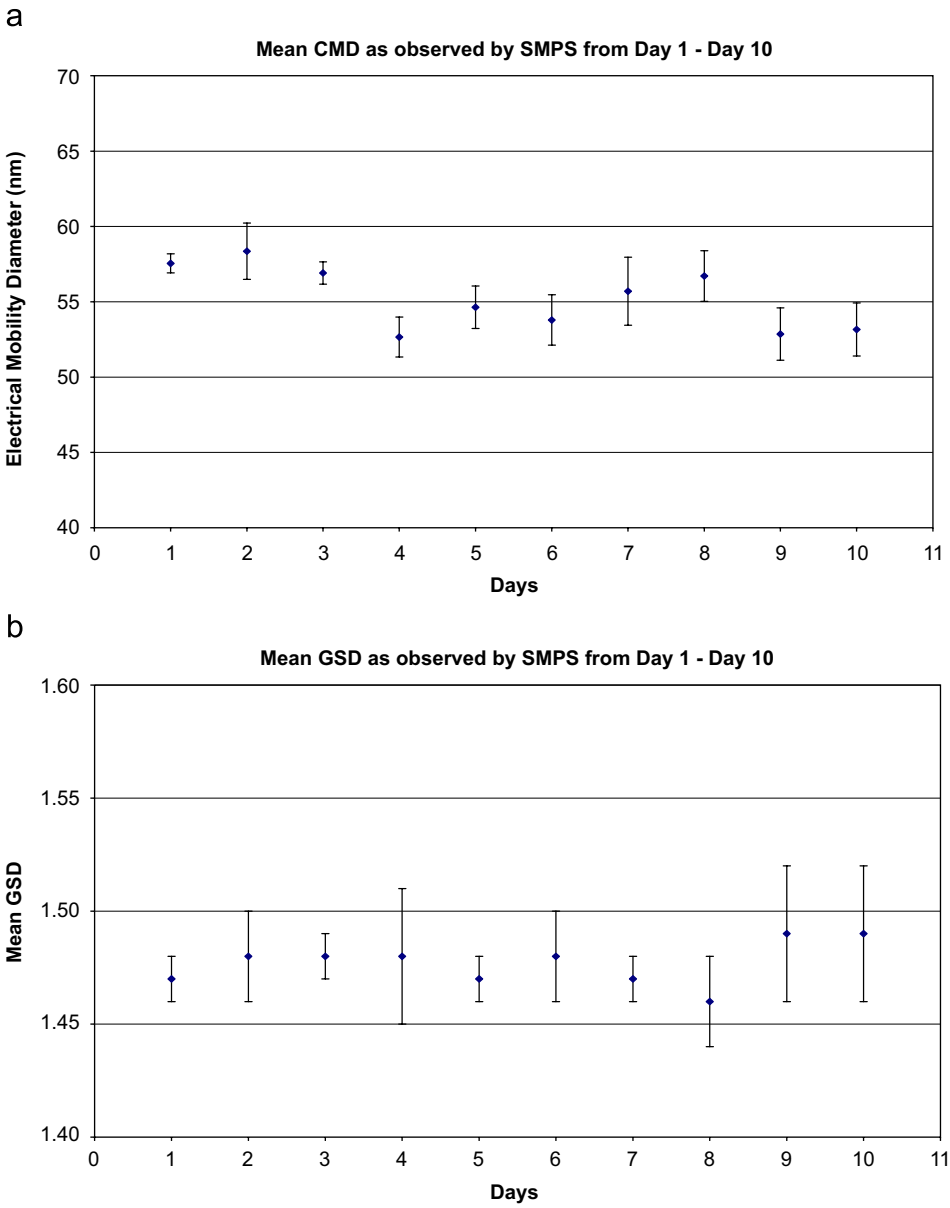

Fig. 3. (a). Mean count median diameter, as recorded by SMPS, during a 3-h period for a 10-day test generation. (b). Geometric standard deviation, as recorded by SMPS, during a 3-h period for a 10-day test generation.

lacy carbon-coated copper grid. The samples were collected over a 5-min period to deposit a thin uniform coating of test material on the grid. The microscope is fitted with a LaB_6 filament and an ultra-high-resolution pole piece. With the acceleration voltage at 200 keV, the point-to-point resolution of 0.194 nm was achieved, suitable for high resolution structural imaging. The compositional analysis software used was an INCA X-ray energy spectroscopy system from Oxford Instruments. Five images of the grid were taken at 25 k× magnification to include a sufficient number of particles for size analysis. These images were analyzed for quantitative particle examination, using a Scion image analysis program (Scion Corp, Frederick, MD) to confirm the particle size to be in the nano-sized ranges (< 100 nm).

The particle size distribution was also determined using a MOUDI impactor. This impactor has 13 rotating stages with nominal cut points varying from 10 nm to 10 μm when operated at an inlet flow rate of 10.0 ± 0.5 lpm. The samples were collected on aluminum foil placed at each stage, for a period of 20 min. The mass loadings on each stage

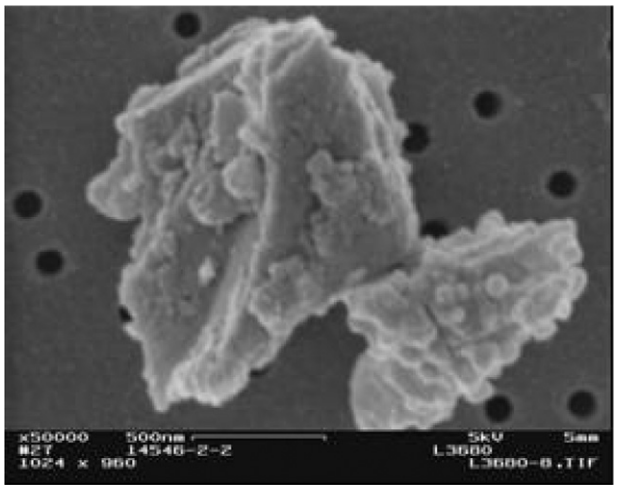

Fig. 4. SEM image of the bulk C_{60}.

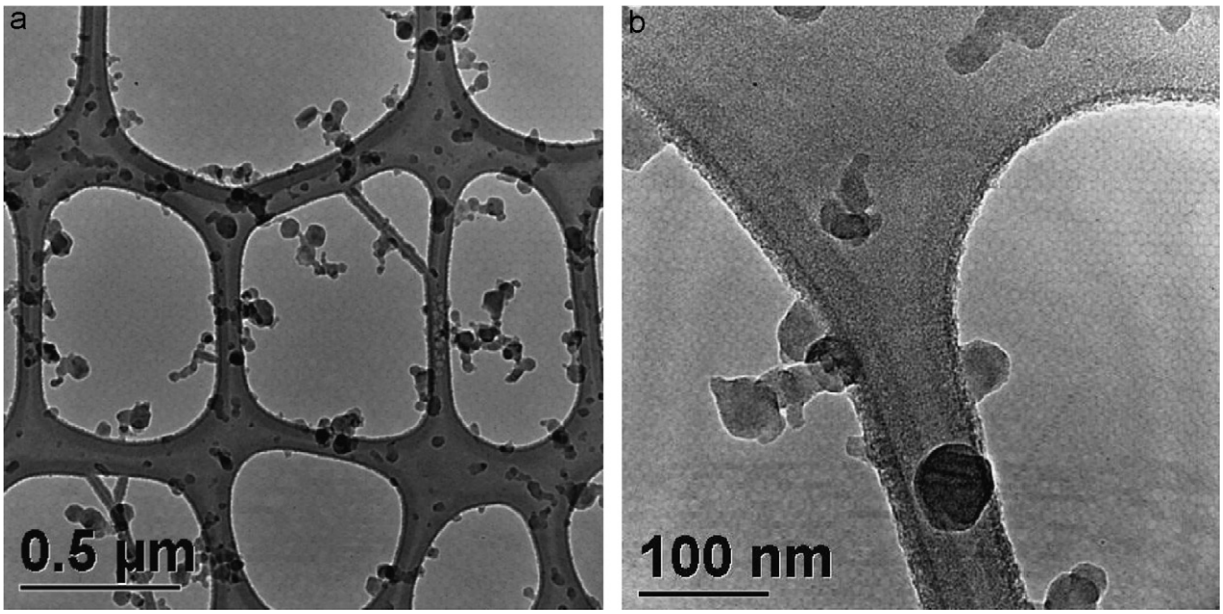

Fig. 5. TEM images of the nano-sized C_{60} sample at two different resolutions.

were determined using gravimetric analysis (UMX-2, Mettler-Toledo, Columbus, OH). The C_{60} powder bulk density of 0.65 g/cc was used to convert mass median diameter (MMD) to mass median aerodynamic diameter (MMAD). The count median diameter (CMD) was calculated from the MMAD using the geometric standard deviation (GSD) of the particle size distribution, and the results were compared to the CMD obtained from the SMPS analysis.

Laser Raman spectroscopy, XRD and HPLC were used to establish the chemical purity of the test material at the nose port of the exposure carousel. Laser Raman spectra were obtained in the backscatter configuration using a Spex Raman spectrometer (Edison, NJ, Model 1877) equipped with a Princeton Instruments (Trenton, NJ) liquid-nitrogen-cooled charge-coupled device detector. The 488.0-nm line of Argon Ion Laser (Coherent, Santa Clara, CA, Innova 307) was used for excitation. The laser power was reduced to ∼5 mW using a combination of filters and beam chopping to prevent sample burning. Slit width was 400 µm, and the exposure time was 500 s for most measurements. Spectra were corrected by subtracting the background spectrum of the filter paper.

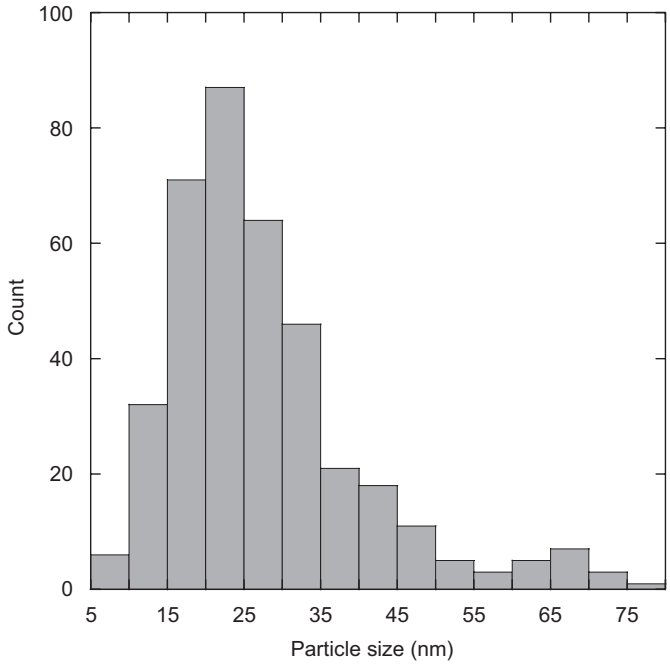

Fig. 6. Histogram obtained using the Scion imaging software applied on TEM images.

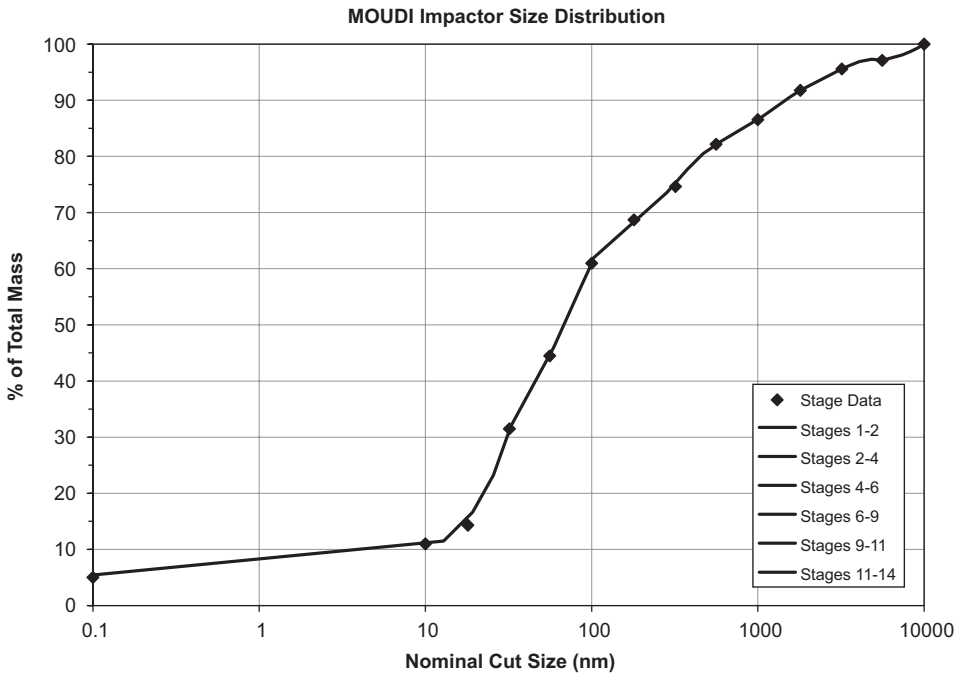

Fig. 7. Representative MOUDI mass distribution.

XRD analysis was performed using a Siemens D5000 θ/θ diffractometer using Cu radiation at 40 kV/30 mA. Scans were run over the range of 5°–80° with a step size of 0.02°. The scan time was 10 h for the bulk powder sample, while the filter samples of nanoparticles were run for 36 h each. The nanoparticle filter samples were run for a longer duration because of small mass deposited on the filter as compared to the bulk powder sample. The phase identification

Table 2
Effects of furnace temperature on the particle size and chemistry at a constant aerosol flow rate through the furnace

Furnace temp. (°C)	Particle size (nm)	Particle conc. (μg/L)	Purity results[a]	Conclusions
500	50–60	2	Pure C_{60}	Some larger particles also observed
550	50–60	2	Pure C_{60}	Negligible larger particle observed (< 0.3% N)
600	40–50	1.5–2	~90–95% C_{60}	Smaller particles but some graphitization observed
650	40–50	1.5–2	~80–95% C_{60}	Smaller particles but some graphitization observed
700	30–40	1.0–1.5	~50–70% C_{60}	Smaller particles, decreased mass conc. with a lot of graphitization
800 +	20–35	0.5–1.5	< 50% C_{60}	Smaller particles, decreased mass concentration, increased number concentration, impure C_{60}

[a]As determined by the comparison of gravimetric and HPLC analysis on filter samples.

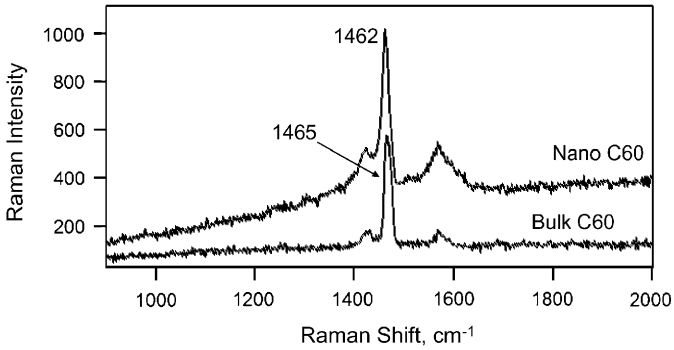

Fig. 8. Raman spectrum of bulk and nano-sized C_{60}.

was accomplished by matching the peak positions and intensities with those listed in the powder diffraction file (PDF) published by the International Center for Diffraction Data (Newtown Square, PA). As a further test of the phase purity, Rietveld refinement was performed on the samples. The Rietveld refinement used a commercial program Jade v7.5 (Materials Data Inc.) and a Lorentzian peak profile.

HPLC analysis of the C_{60} sample was performed using an Agilent 1100 high-pressure liquid chromatograph equipped with an Agilent 1100 variable wavelength detector. The detector was configured at a wavelength of 330 nm and a peak width of >0.1 min. The isocratic separation method involved a 5-μL injection onto a Cosmosil BuckyPrep analytical column (25 cm × 4.6 mm ID; 5 μm) with toluene as the mobile phase. The flow rate of the mobile phase was set at 1 mL/min with a run time of 20 min; retention time for the C_{60} was ~8 min. The samples were collected on a membrane filter that was analyzed gravimetrically and then dissolved in toluene to extract C_{60}. The HPLC analysis on this solution indicated the total mass of C_{60} present on the filter. This mass was compared to the gravimetric mass recorded earlier to detect the presence of impurities on the filter sample.

3. Results and discussion

The SMPS was used to monitor the nanoparticle size distribution and demonstrated that the vaporization condensation process was able to reliably and reproducibly generate C_{60} aerosol with a count median size ranging from 40 to 60 nm. Table 1 summarizes typical aerosol size data for a 3-min sampling period during the stable generation of aerosol. A CMD of 53 nm with a GSD of 1.53 was observed. The total particle number concentration was ~8.20×10^6 particles/cc. This total number concentration has been adjusted to account for the dilution of

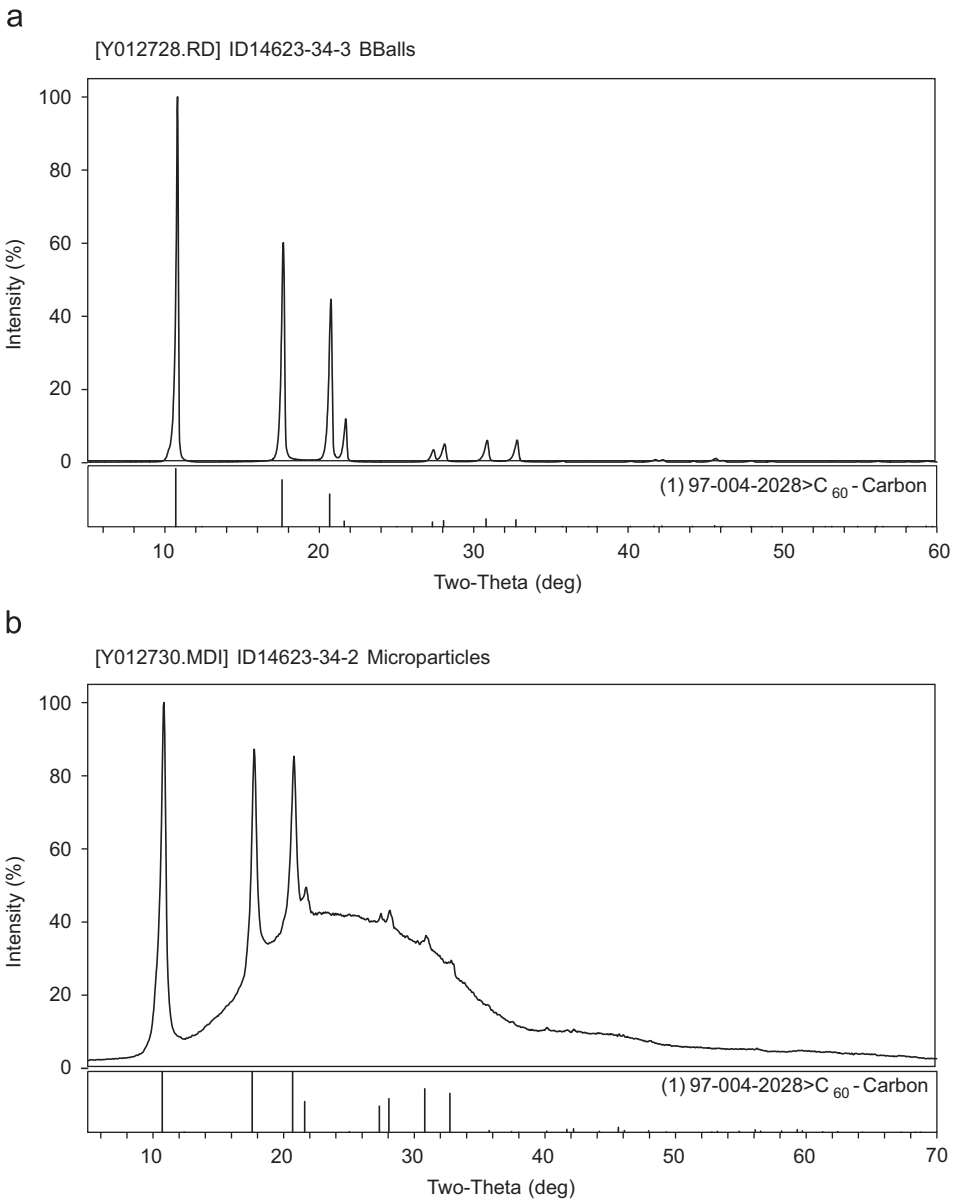

Fig. 9. (a). XRD spectrum obtained using bulk C_{60} material for phase identification. (b). XRD spectrum obtained using nano-C_{60} filter sample for phase identification.

the sample flow at the inlet to the SMPS. Fig. 2 demonstrates a typical particle number-based distribution during a 3-min sample period. SMPS analysis showed that >99.7% of the total particles were < 100 nm electrical mobility diameter.

Fig. 3 shows the consistency of generation during 10 consecutive days as measured by SMPS. Each data point is the mean of 3 h of generation. Fig. 3(a) shows the mean CMDs, recorded by SMPS, during the 3-h test generated each day for a 10-day test generation period. Fig. 3(b) shows the geometric standard deviation of the particle size distribution for the same period as recorded by the SMPS.

SEM images of the bulk material were taken to establish the initial size of the feed material. Fig. 4 shows the SEM image of the C_{60} bulk material as collected at the output of the PAC. The TEM samples of the nano-sized C_{60} samples were collected from the nose port of the exposure carousel. Fig. 5 shows the TEM images of the nano-sized aerosol

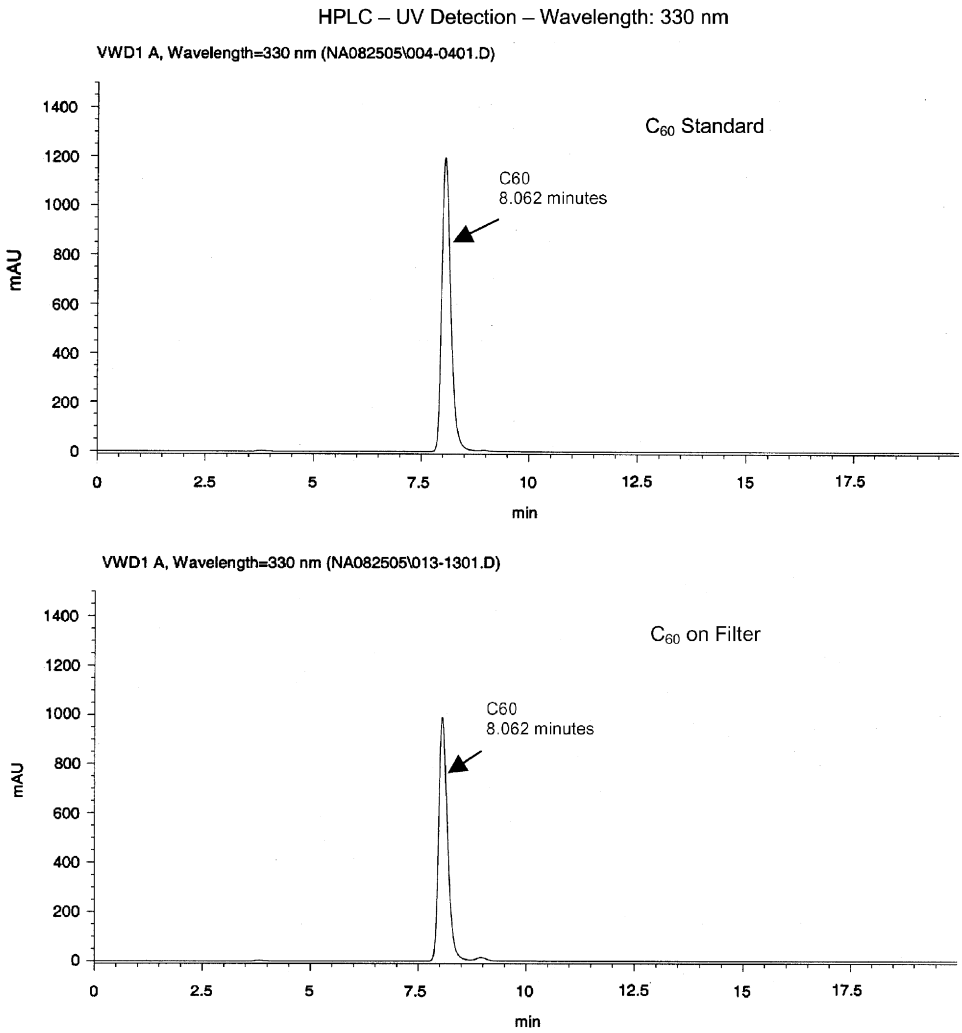

Fig. 10. Representative HPLC chromatograms of C_{60} standard and sample.

filter samples at two different magnifications. The particle size looked consistent with the SMPS size distribution. Fig. 6 shows the software-resolved (Kaleidagraph, Synergy Software, Reading, PA) histogram obtained using the imaging software. The mean particle size was ~25 nm, thus confirming that the actual physical size of the particles were in nano-sized ranges (< 100 nm). This particle size may be different from the mean aerosol electrical mobility size observed by SMPS as the number of particles analyzed in the imaging software were orders of magnitude lesser than those observed in SMPS.

The MOUDI impactor analysis determined the mass size distribution of the generated nanoparticles. Fig. 7 shows the cumulative mass distribution as the function of particle size obtained using the MOUDI impactor. The MMAD of 58 nm was calculated using the MOUDI impactor analysis. Using the GSD range of 1.40–1.50, the range of the CMD for this particle size distribution was calculated as 44–51 nm aerodynamic size. These results agreed fairly well with CMDs obtained using SMPS, and the comparison results were in good agreement with previous reported work (Sioutas, Abt, Wolfson, & Koutrakis, 1999).

Some previously reported literature has suggested that C_{60} powder decomposes to amorphous/black carbon at temperatures >700 °C (Mochida, Egashira, Korai, & Yokogawa, 1997). Therefore, C_{60} samples, collected at the nose port of the exposure carousel, were subjected to extensive chemical characterization to determine whether the nanoparticle generation process modified the chemical composition of C_{60} nanoparticles as compared to the bulk C_{60} powder.

Table 2 summarizes the effects of increasing furnace temperature on the size and chemical integrity of C_{60} fullerene particles at a constant aerosol flow rate of 400 mL/min through the furnace tube. At lower temperatures (< 500 °C), the samples taken at the nose port of the exposure carousel were pure C_{60}, but the observed particle sizes of the aerosol were larger (CMD>100 nm). At higher temperatures (>600 °C), C_{60} started decomposing into amorphous carbon, as the presence of certain impurities was evident by HPLC and Raman analysis. At very high temperatures (>800 °C), a lot of amorphous carbon (>50% by weight) was detected on the filter, and the number concentration was so high ($>10^7$ particles/cc) that it exceeded the operating range of the SMPS.

Fig. 8 shows the Raman spectra obtained using nano-sized and bulk C_{60} material. The Raman spectra for both samples look identical. No presence of graphitic/amorphous carbon was observed. A small shift in the frequency of the peak in the nano-sized sample was observed, that may be caused by overheating of the sample by the laser beam, which typically causes the shift of Raman bands to lower frequencies.

Fig. 9 shows the experimental patterns obtained using XRD on the bulk and nano-sized C_{60} samples. The relative intensity of peaks observed in the nano-sized filter sample were an order of magnitude less than the same peaks for the bulk powder sample because of the small amounts of nano-sized C_{60} collected on the filter. The only crystalline phase detected was the face-centered cubic form of C_{60} with Fm-3m symmetry (SG = 225). No other phase of carbon could be detected thus confirming the purity of C_{60} samples. The Rietveld refinements further confirmed the purity of the crystalline component as no other crystalline phase was detected on the filter samples. The residual peaks showed no extra peaks and only minimal errors concentrated at the strong peaks. The resulting residual error was $R_{wp} = 12.03\%$.

HPLC was used to further characterize the chemical purity of C_{60} bulk material and generated nanoparticles. Fig. 10 shows a typical HPLC chromatogram obtained using C_{60} standard and the filter sample collected. A big peak was observed in the chromatogram of nano-sized C_{60} filter sample, the location of which agreed fairly well with the peak location in the C_{60} standard chromatogram. The ratio of gravimetric mass to the HPLC determined C_{60} mass was observed to be close to 1, thus suggesting that there was nothing besides C_{60} collected on the filter sample.

4. Conclusions

We have developed an aerosol generation system that can produce C_{60} nanoparticles at a mass concentration >20 times higher than previously reported (Gurav, Kodas, Wang, Kauppinen, & Joutsensaari, 1994). Several experiments were conducted to optimize the operating parameters of the generation system. As discussed earlier, the temperature of the furnace tube was optimized to ensure the chemical integrity of C_{60} aerosol. At higher temperatures, the chemical decomposition of C_{60} to black/amorphous carbon was evident, whereas at lower temperatures, particle size may be too big. Similarly, the flow rate of the aerosol in the furnace tube was optimized to ensure enough residence time for complete vaporization of the large particles. At lower flow rates, the residence times may be too high and the particle agglomeration may result in bigger particle sizes, whereas at higher flow rates, the residence times may be too low and bigger particles may not vaporize. The dilution nitrogen gas introduced inside the furnace tube helped in achieving super-saturation conditions and reducing the residence time during the condensation of the C_{60} vapor molecules. The rigorous physical size and chemical characterization methods we have employed have shown that nanoparticles can be generated in a defined size range reproducibly without altering the chemical composition of the particles. The particle size of the aerosol, as measured by different techniques, seemed to agree fairly well with each other. Also, the C_{60} nanoparticles were generated in an exposure atmosphere that is conducive to perform the inhalation health and safety testing of C_{60} nanoparticles.

References

Borm, P. J. A., Robbins, D., Haubold, S., Kuhlbusch, T., Fissan, H., Donaldson, K. et al. (2006). The potential risks of nanomaterials: A review carried out for ECETOC. *Particle and Fibre Toxicology*, *3*(11),

Cheng, M.-D. (2004). Effects of nanophase materials (< = 20 nm) on biological responses. *Journal of Environmental Sciences and Health*, *39*(10), 2691–2705.

Colvin, V. L. (2003). The potential environmental impact of engineered nanomaterials. *Nature Biotechnology*, *21*, 1166–1170.

Damour, T. M., Ehrman, S. H., Karlsson, M. N. A., & Karlsson, L. S. (2005). Experimental evidence for nonuniform flow in a horizontal evaporation/condensation aerosol generator. *Aerosol Science and Technology*, *39*, 444–451.

Gerritzen, G., Huang, L.-C., Killpack, K., Holden, P., & Harthorn, B. H. (2006). Review of safety practices in the nanotechnology industry. Phase one report prepared for the International Council on Nanotechnology by the University of California, Santa Barbara, October 18.

Gurav, A. S., Kodas, T. T., Wang, L.-M., Kauppinen, E. I., & Joutsensaari, J. (1994). Generation of nanometer size fullerene particles via vapor condensation. *Chemical Physics Letters*, *218*, 304–308.

Hood, E. (2004). Nanotechnology: Looking as we leap. *Environmental Health Perspectives*, *112*(13), A740–A749.

Joutsensaari, J., Ahonen, P., Tapper, U., Kauppinen, E. I., Laurila, J., & Kuokkala, V. T. (1996). Generation of nano phase fullerene particles via aerosol routes. *Synthetic Metals*, *77*, 85–88.

Kreuter, J. (2001). Nanoparticulate systems for brain delivery of drugs. *Advanced Drug Delivery Reviews*, *47*, 65–81.

Kroto, H. W., Heath, J. R., O'Brien, S. C., Curl, R. F., & Smalley, R. E. (1985). C60: Buckminsterfullerene. *Nature*, *318*, 162.

MacNee, W., & Donaldson, K. (2000). How can ultrafine particles be responsible for increased mortality?. *Monaldi Archives for Chest Disease*, *55*, I35135–I39139.

McCready, D. E., & Alnajjar, M. S. (1993). Powder data for Buckminster fullerene, C_{60}. *Powder Diffraction*, *9*(2), 93–95.

Meili, C. (2006). A multi-stakeholder-dialogue-approach towards a sustainable regulatory framework for nanotechnologies and nanosciences. A report prepared by The Innovation Society Ltd., March 2006.

Mochida, I., Egashira, M., Korai, Y., & Yokogawa, K. (1997). Structural changes of fullerene by heat treatment up to graphitization temperature. *Carbon*, *35*(12), 1707–1712.

Oberdorster, G. (1996). Significance of particle parameters in the evaluation of exposure dose response relationships of inhaled particles. *Particle Science and Technology*, *14*, 135–151.

Oberdorster, G., Maynard, A., Donaldson, K., Castranova, V., Fitzpatrick, J., Ausman, K. et al. (2005). Principles for characterizing the potential human health effects from exposure to nanomaterials: Elements of a screening strategy. *Particle and Fibre Toxicology*, *2*(8),

Oberdorster, G., Oberdorster, E., & Oberdorster, J. (2005). Nanotoxicology: An emerging discipline evolving from studies of ultrafine particles. *Environmental Health Perspectives*, *113*(7), 823–839.

Sioutas, C., Abt, E., Wolfson, J. M., & Koutrakis, P. (1999). Evaluation of the measurement performance of the scanning mobility particle sizer and aerodynamic particle sizer. *Aerosol Science and Technology*, *30*, 84–92.

Taylor, R. M. (2006). Regulating the products of nanotechnology: Does FDA have the tools it needs? A report from the Project of Emerging Nanotechnologies, October.

The National Nanotechnology Initiative. (2006). Environmental, health and safety research needs for engineered nanoscale materials. A report prepared by National Science and Technology Council, Committee on Technology and Nanoscale Science, Engineering and Technology Subcommittee.